Journal of Materials Chemistry A

Accepted Manuscript

ROYAL SOCIETY OF CHEMISTRY

www.rsc.org/materialsA

Journal of Materials Chemistry A

Cite this: DOI: 10.1039/

www.rsc.org/materilas

Paper

Tailoring Molecular Architectures of Fe Phthalocyanine on Nanocarbon Supports for High Oxygen Reduction Performance

Shiming Zhang, Heyou Zhang, Xing Hua, Shengli Chen*

Received (in XXX, XXX) Xth XXXXXXXXX 20XX, Accepted Xth XXXXXXXXX 20XX

DOI: 10.1039/b000000x

Abstract. Cost-effective non-precious metal electrocatalysts for the oxygen reduction reaction (ORR) is the key for fuel cells to become a viable electricity generation technology. Metal macrocyclic compounds such as Fe/Co porphyrins and phthalocyanines are excellent molecular catalysts for O_2 reduction; but they are still considerably less competitive than Pt-based materials when catalyzing the ORR in electrochemical environments. Using Fe phthalocyanine (FePc) as a mode compound, we show that the electrocatalytic activity of metal macrocyclic compounds for the ORR can be greatly enhanced through tailored assembling architectures on high-surface-area nanocarbons. By simply ball-milling FePc with nanocarbons such as graphene nanosheets and carbon-black nanoparticles, molecular architectures of FePc from nanorods to uniform thin shells are obtained. The resulted carbon-supported FePc composites exhibit ORR performance much superior to the state-of-the-art carbon-supported Pt in alkaline solution, with up to 60 mV positive shift in the half-wave potential and more than 5 times increase in the mass activity. As well as showing that the molecule-support interaction provides a degree of control on the molecular architectures of metal macrocyclic compounds, the present work reveals that the FePc molecule is intrinsically much more efficient than Pt in catalyzing the ORR in alkaline media, and therefore has great prospect as cathode electrocatalyst in alkaline fuel cells.

1. Introduction

Owing to the high power density and energy yield and the low environmental impact, fuel cells have attracted increasing attention as candidates for electricity generation technologies in the sustainable society. One of the major bottleneck for large scale application of fuel cells is the demand for Pt to catalyze the sluggish oxygen reduction reaction (ORR) at the cathode.[1-3] As well as the scarcity, Pt-based materials as ORR electrocatalyst also suffer from activity decline due to

the relatively low instability under the harsh oxidizing condition of ORR and the poor tolerance to the poisoning molecules such as methanol. Therefore, non-previous-metal catalysts (NPMCs) for the ORR are highly desired.[4, 5]

Porphyry type of metal-nitrogen (Me-N) macrocyclic complexes such as Fe/Co porphyrins and phthalocyanines have long been known as excellent molecular catalysts for O_2 reduction. Since Jasinski's finding in 1964 that Co phthalocyanine could catalyze the ORR in alkaline solution,[6] a diverse range of NPMCs ORR electrocatalysts based on Me-N macrocyclic complexes have been demonstrated in the literature.[7-23] As compared with Pt-based materials, however, most of these electrocatalysts are much less efficient in electrochemical environments. Conventionally, high temperature (HT) treatments have been generally used to improve the electrocatalytic activity of Me-N macrocyclic complexes.[9-13] The complex decomposition and reaction of macrocyclic molecules during the HT treatments make it extremely difficult to tailor the structure and surface properties of the resulting materials. Therefore, the nature of the actual catalytic sites in these materials has been in debate, which inhibits the rational structural and morphological desire of Me-N based electrocatalysts.

Recently, non-pyrolyzing preparation of Me-N complex electrocatalysts have received increasing interests.[14-24] Especially, it has been shown that the composites of Me-N macrocyclic complexes supported on various novel nanocarbons such as graphene and carbon nanotube (CNT) can efficiently catalyze the ORR. In addition to efficiently transport electrons involved in the electrocatalytic processes, the nanocarbons allow effective dispersion and assembly of the Me-N macrocyclic molecules due to their high surface areas and the unique molecule-support interactions. The latter may also result in favorable electronic modification of Me-N macrocyclic molecules,[24-26] thus maximizing the electrocatalytic activity. So far, the reported Me-N complex/carbon composites with excellent ORR activity were mostly constructed using relatively complicated methods, for examples, axial ligand tethering[17], layer-by-layer assembly[18] and covalent grafting[19]; while simple mixing usually led to ORR performance much inferior to Pt-based materials,[20-23] probably due to the relatively weak molecule-support interaction.

In this work, we show that composites of phthalocyanine (FePc) on nanocarbons with superior ORR activity can be fabricated using a simple wet ball-milling method (see experimental section). Ball-billing is among the straightforward and efficient methods to prepare composite materials. Recently, it has been widely employed, or combined with HT pyrolysis, to prepare doped carbons to catalyze the ORR.[11-13, 27] The ball-billing were shown to significantly increase the effective catlytic sites in doped carbons.[11-13] The direct ball-billing preparation of ORR electrocatalysts of

carbon-supported Me-N macrocyclic complexes has been rarely reported. The high-speed ball-milling not only allows efficient blending of carbon supports and macrocyclic complexes, but could also result in enhanced molecule-support interaction. Besides, the relatively low-temperature preparation should avoid destroying the Me-N coordination structure. More importantly, the results in this work show that the assembling behaviors of FePc molecules in the ball-milling processes, and accordingly the electrocatalytic activity of the resulted composites, can be modulated by using different nanocarbons and by varying the FePc/carbon ratios. As illustrated in Scheme 1, a composite of FePc nanorods on graphene nanosheets (GS) can be obtained when FePc is ball-milled together with two dimensional (2-D) GS; as the high-surface-area carbon-black (CB) EC600 (Ketjenblack) are used as supporting materials for FePc, the ball-milling produces a core-shell structured composite, in which FePc is uniformly coated on CB nanoparticles. The two types of composites, denoted as FePc/GS and FePc/CB-EC600 respectively, have greatly enhanced ORR performance over the FePc nanorods produced by ball-milling FePc alone. Furthermore, they are much superior to the state-of-the-art carbon-supported Pt (Pt/C) catalyst in catalyzing the ORR in alkaline solution, therefore showing great prospect as cathode electrocatalyst in alkaline fuel cells.

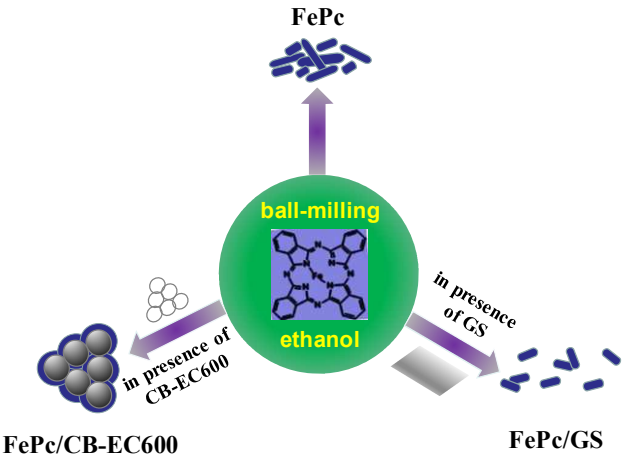

Scheme 1. Schematic illustration of ball-milling preparation of FePc-based catalysts.

2. Results and Discussion

2.1 Morphology and structure characterization of the carbon-supported FePc composites.

The varying assembling architectures of FePc molecules on different nanocarbon supports were revealed by the electron microscopic observation (Fig. 1). The composite FePc/GS exhibited a uniform blending of nanorod-shaped FePc assemblies and GS (Fig. 1a and b). The FePc nanorods were typically ca. 30 nm in radii but somewhat polydisperse in lengths. The ball-milling of FePc alone also produced nanorod assemblies, but they were highly agglomerated (Fig. 1e). The FePc

precursor prior to the ball-milling showed even more severe agglomeration, containing irregular and cumulate blocks with widely varied shapes and sizes (Fig. S1). These results suggested that the ball-milling has helped the self-assembly of FePc molecules into rod-like architectures through inter-molecular π-π interaction. The presence of 2-D GS as supports prevented the nanorods from agglomeration. As shown in Fig. 1c and d, the FePc/CB-EC600 composite retained the particle-aggregation morphology of the CB-EC600 (Fig. 1f). However, no individual FePc nanorod was seen in this composite. This indicated that the use of high-surface-area CB nanoparticles as supporting materials inhibited the π-π stacking of FePc molecules, thus forming a core-shell structured composite in which FePc molecules are adsorbed on EC600 particles.

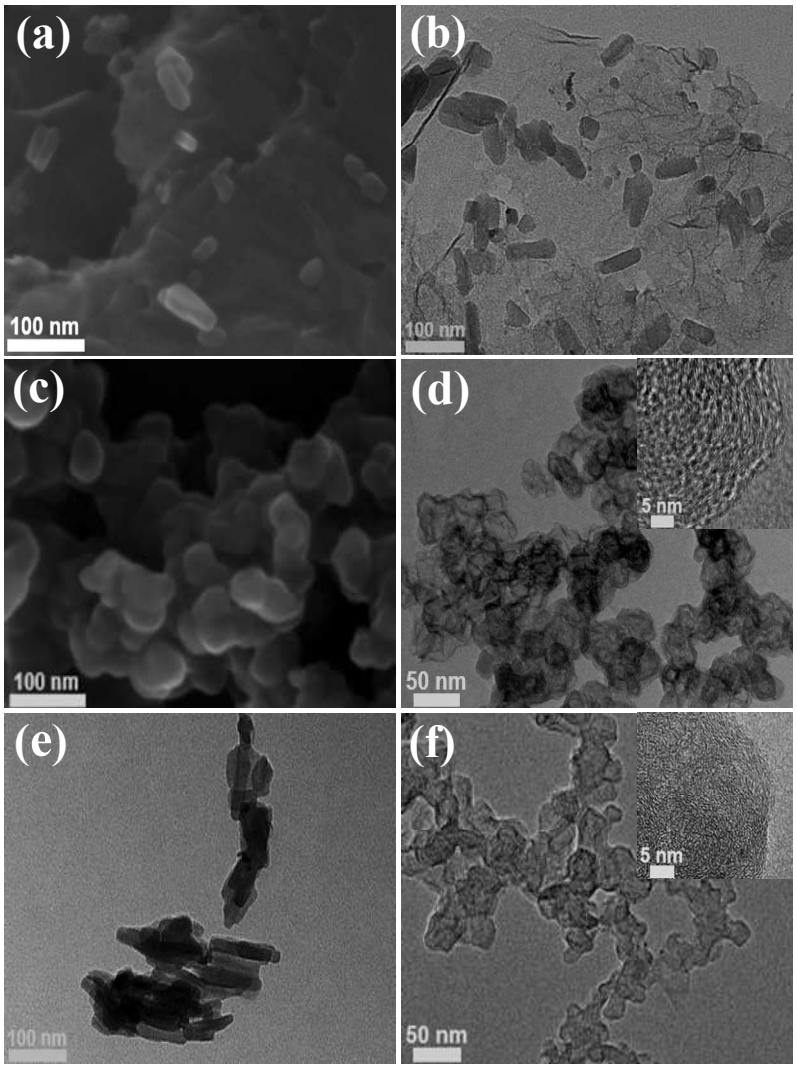

Fig. 1 Morphologies of FePc and carbon-supported FePc composites: (a) SEM and (b) TEM images of FePc/GS composite; (c) SEM and (d) TEM images of FePc/CB-EC600; TEM images of (e) FePc and (f) CB-EC600. The insets of (d) and (f) are the representative high-resolution TEM images of FePc/CB-EC600 and CB-EC600. All images were for samples obtained after ball-milling.

By careful inspecting the TEM images in Fig. 1d and f and the high resolution ones in the insets, one can clearly see the subtle structural differences between FePc/CB-EC600 and CB-EC600. The former contains more curvature and dislocation on the surface, which should be an indication of the presence of FePc shell. To further confirm the core-shell structure of the FePc/CB-EC600 composite, we measured the depth-dependent contents of the main composing elements in the composite, namely, Fe, N and C, using the etching X-ray photoelectron spectroscopy (XPS). As seen in Fig. 2, the atomic content of C increases with the etching time; whereas those of N and Fe decrease nearly simultaneously with time. This indicated that the FePc molecules were mainly located in the surface region of the sample.

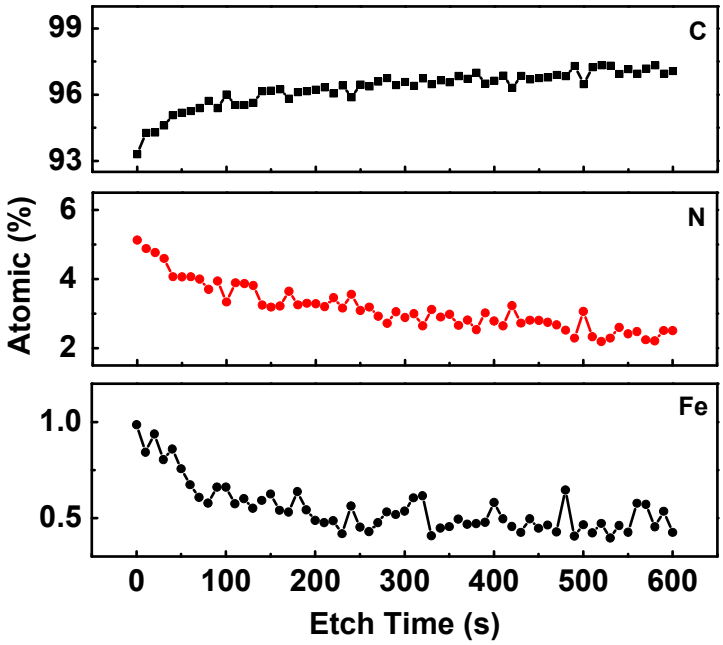

Fig. 2 Etching XPS responses of C, N, and Fe for the FePc/CB-EC600 composite.

The assembling architecture of FePc molecules in a carbon-supported composite should be a result of the molecule-support interaction and molecule-molecule interaction. In the case when the molecule-support interaction is stronger than the molecule-molecule interaction, FePc molecules would first prefer to form a uniform adsorption shell on the surface of nanocarbon materials instead of individual molecular aggregates (e.g., nanorods). As the thickness of FePc adsorption shell increases till the interaction of the support with the FePc molecules in the outer layer is too weak as compared with the molecule-molecule interaction, individual molecular aggregates of FePc would form. As well as the competition between the molecule-support and molecule-molecule interactions, the amounts of adsorbed FePc depend on the specific surface area of the supporting material. Approximately, a monolayer adsorption of FePc on CB-EC600 requires a

FePc/carbon mass ratio of ca. 1:2 if assuming that all the BET surface areas of carbon support (~1300 m^2/g for Ketjenblack EC600) are available for FePc (a monolayer of FePc approximately have a surface density of 4-5×10^{-4} g/m^2). When preparing the composites shown in Fig. 1, a FePc/carbon mass ratio of 1:1 was used, which corresponded to a two-layer adsorption of FePc molecules on CB-EC600 particles. This seemed to suggested that the molecule-support interaction in FePc/CB-EC600 composite is much stronger than the inter-molecular interaction of FePc.

To test the effects of the specific surface areas and FePc/carbon ratios on the assembling behaviors of FePc molecules in the composites, we made composites by ball-milling of FePc with CB particles of XC-72R, which has much lower BET surface area (~250 m^2/g) than the CB-EC600 (~1300 m^2/g). With the FePc/carbon mass ratio of 1:1, the resulted composite exhibited a morphology of mixture of agglomerated FePc nanorods and CB particle aggregates (Fig. S2a in supporting information). Similar morphologies were also observed for FePc/CB-EC600 composites with FePc/carbon mass ratios much larger than 1:1 (Fig. S2b).

The GS used in present study had a specific surface area of ~680 m^2/g, on which a monolayer of FePc corresponds to a FePc/carbon mass ratio of ca. 1:4. If the molecule-support interaction in FePc/GS composites is similar to that in FePc/CB-EC600 composites, one would expect that no individual FePc nanorod forms as the mass ratio is below ca. 1:2. However, FePc nanorods were found even in FePc/GS composites with FePc/carbon mass ratios down to 1:4 (Fig. S3). This suggested the molecule-support intercation between FePc and GS is considerably weaker than that between FePc and CB particles. Therefore, FePc molecules in FePc/GS composites prefer to be self-assembled into nanorod aggragates. However, GS as support prevented the FePc nanorods from agglomerating. In addition, GS should also efficeintly transport the electrons involved in the electrocatalytic processs. The much stronger molecule-support intercation in FePc/CB-EC600 composites may be related to the highly porous structure of the supporting material.

The different assembling architectures of FePc molecules in the FePc/CB-EC600 and FePc/GS composites were also manifested by the X-ray diffraction (XRD) results (Fig. 3). The XRD peak at 2θ value of ca. 7° was believed to be a characteristic response of the molecular aggregates of FePc.[28] This peak was sharp in the spectra for the FePc/GS composite and pure FePc; whereas it became obviously broadened in the XRD pattern for the FePc/CB-EC600 composite, suggesting that FePc molecules in the latter were less aggregated. In addition, the XPS results (Fig. S4) showed that the surface contents of N and Fe in the FePc/CB-EC600 composite were considerably lower than that in the FePc/GS composite and FePc (Table S1), which should also be an implication for the higher dispersion of FePc in the FePc/CB-EC600 composite.

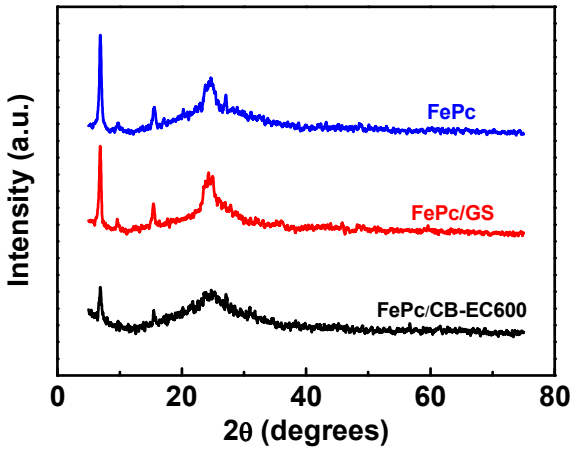

Fig. 3 XRD patterns of FePc/CB-EC600, FePc/GS, and FePc.

Fig. 4 compares the UV-Vis absorption spectra of the FePc/CB-EC600, FePc/GS and FePc in ethanol solution. The pure FePc exhibited the characteristic B-band at 329 nm that corresponded to the electron transition from a_{2u} and b_{1u} to e_g* orbitals and G-band at 639 nm that was caused by the π-π* transition of FePc ring.[24] It can be seen that the absorption peaks for FePc became obviously weak in the two composites. As shown in the inset of Fig. 4, obvious bathochromic shifts of the G-band, to ~660 nm for FePc/GS and 665 nm for FePc/CB-EC600 respectively, occurred for the two composites. This should be an indication of the strong electronic coupling between FePc and carbon supports. In addition, a closer look revealed the existence of a weak absorption peak at ~565 nm in FePc/GS that was clearly seen in the spectra for FePc; whereas it was absent in that for the FePc/CB-EC600. This suggested that the peak at ~565 nm was due to the aggregation of FePc.

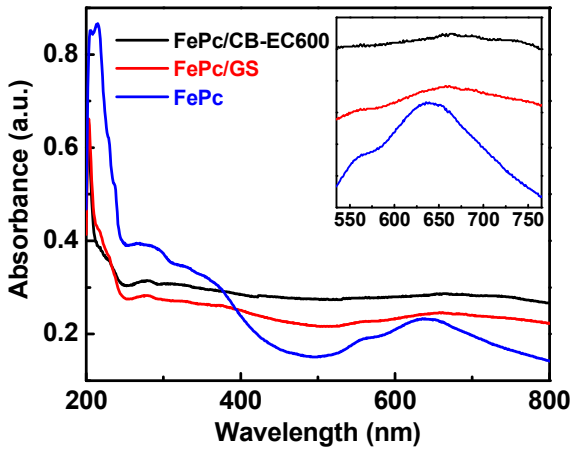

Fig. 4 UV-Vis absorption spectra of FePc/CB-EC600, FePc/GS, and FePc in ethanol. The inset is the enlarged spectra between 535 nm and 765 nm.

The electronic interaction between FePc and carbon supports was also suggested by the XPS results (Fig. S4b and c). The FePc/CB-EC600 composite exhibited binding energy shift of ca. 0.3

and 0.9 eV respectively for N and Fe as compared to the pure FePc; while the corresponding shifts were ca. 0.1 and 0.5 eV respectively for the FePc/GS composite. This suggested that there was significant electron donation from the FePc molecules to the carbon supports, especially in the FePc/CB-EC600 composite.

2.2 ORR performance of the carbon-supported FePc composites

The ORR performance of the carbon-supported FePc composites were compared with the pure FePc and the commercial Pt/C (20 wt %, Johnson-Matthey) through rotating ring-disk electrode (RRDE) measurements in 0.1 M KOH saturated with O_2. The RRDE consisted of a glass carbon (GC) disk electrode and a Pt ring electrode. The ORR took place on the GC disk electrode (5 mm diameter), on which the catalyst sample was deposited as a thin film with the usual ink casting method (Experimental Section); while on the ring electrode the peroxide produced on disk electrode during O_2 reduction was oxidized to water.

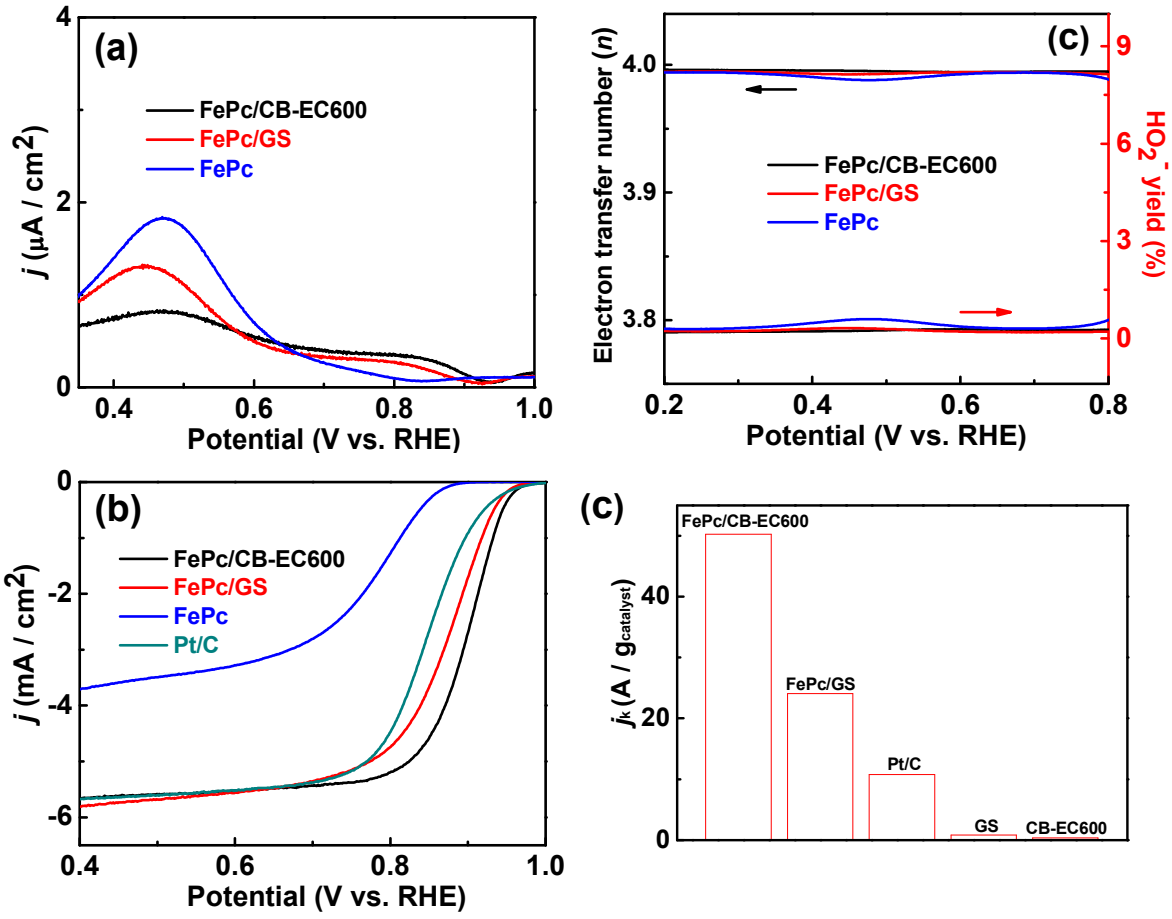

Fig. 5 ORR performance comparison: (a) and (b), the ring and disk currents as functions of the disk electrode potential obtained in steady-state polarization measurements using a potential sweeping rate of 5 mV/s; (c), the effective electron transfer number (n) and H_2O_2 yields in ORR on various electrocatalysts estimated from the corresponding ring currents; (d), the mass activities at 0.9 V (vs. RHE). Catalyst loading: 0.1 mg/cm^2.

According to the ratios between the currents measured on the ring (Fig. 5a) and disk (Fig. 5b) electrodes, the yields of peroxide and the effective electron numbers in the ORR at different potentials (Fig. 5c) were estimated (Eq. 1 and 2, experimental section). One can see that the FePc and two carbon-supported FePc composites exhibited very low peroxide yields over the potential range from 0.2 to 0.8 V (versus the reversible hydrogen electrode, RHE). Accordingly, the effective electron transfer numbers (n) in the O_2 reduction were very close to 4. The polarization curves measured with different electrode rotation rates and the corresponding Koutecky-Levich (K-L) plots (Fig. S5) at a variety of potentials similarly suggested that the FePc-based electrocatalysts in this study catalyzed the ORR through the 4-electron reaction pathway similar to that on Pt/C. The n values estimated from the K-L plots for the two composites were both ca. 3.99.

As shown by the steady-state polarization curves in Fig. 5b, the unsupported FePc aggregates (nanorods) exhibited rather poor ORR performance as compared with the Pt/C; whereas the two carbon-supported FePc composites (1:1 FePc/carbon mass ratio) both showed higher ORR activity than the Pt/C, as indicated by the significant positive shift of the half-wave potentials ($E_{1/2}$). It is worth mentioning that we used the same mass loading of 0.1 mg/cm^2 on the RDE substrate for all the catalyst samples, so that the absolute performance per mass of catalyst can be straightforwardly compared. The FePc/GS and FePc/CB-EC600 exhibited $E_{1/2}$ values of ca 0.88 and 0.91 V respectively, which were 30 and 60 mV more positive than that exhibited by the 20 wt % Pt/C (ca. 0.85 V). In supporting information, we display the ORR performance (positive shift of $E_{1/2}$ as compared with Pt/C) of other carbon-supported Me-N composites which have been reported to exhibit excellent ORR performance in recent literatures (table S2). We noted that in some of these works the ORR performance of Pt/C was not optimized. Despite, the 60 mV positive shift of $E_{1/2}$ for the FePc/CB-EC600 as compared with that of Pt/C remains among the best performance reported so far. We also measured the ORR performance of the pristine carbon supports, namely, GS and CB-EC600 (Fig. S6). In comparison with the corresponding composites, the ORR activities of the pure supports were considerably poor.

Fig 5d displays the mass activities (MA) of various samples at 0.9 V, which were obtained by normalizing the transport-corrected kinetic current (supporting information, Eq. S1) with the mass of the corresponding catalyst sample on the disk electrode. We didn't correct the IR drop when calculating the kinetic current. The MA values for the FePc/CB-EC600 and FePc/GS composites were about 5 and 2.2 times higher than that for the Pt/C respectively. The MA values for the pure GS and EC-600 were negligibly small as compared with the composites and Pt/C. If the intrinsic activities of the active components (FePc and Pt) were considered, the MA of FePc in the FePc/GS

was close to that of Pt in the Pt/C, while the MA of FePc in the FePc/CB-EC600 was about 2 times higher than that of Pt in the Pt/C. This indicated that the FePc molecule is intrinsically more efficient than Pt in catalyzing the ORR. The high intrinsic activity can be realized through effective dispersion on high surface areas supports which may also provide appropriate molecule-support interactions. For molecular catalysts, the turnover frequency (TOF), which refers to the activity per catalytic center, is usually used to measure their catalytic ability. Therefore, we compared the ORR activity of the carbon-supported FePc composites with that of Pt/C by calculating the currents derived by each Fe center in the FePc composites and each surface Pt atom in Pt/C. The obtained values were 20.47×10^{-20} A/(Fe atom) for FePc/CB-EC600 and 9.065×10^{-20} A/(Fe atom) for FePc/GS, both of which were higher than the value of 4.105×10^{-20} A/(surface Pt atom) for Pt/C. This also indicated that the FePc molecule has higher intrinsic catalytic ability than Pt. When calculating the TOF for surface Pt atoms, we have used a mean particle size of 3 nm for the Johnson-Matthey's 20 wt% Pt/C.[29]

We found that reducing the FePc/carbon mass ratio from 1:1 to 1:2 in the FePc/CB-EC600 composites only slightly decreased the ORR activity (Fig. S7). According to the analysis mentioned above, a FePc/carbon mass ratio of 1:2 in the FePc/CB-EC600 composite approximately corresponds to a monolayer adsorption of FePc on CB particles. Thus, it seemed that roughly one monolayer of FePc on CB particles is necessary and also enough to achieve the best ORR activity. For the FePc/CB-EC600 composite with 1:2 FePc/carbon mass ratio, the MA of the FePc was close to 3 times of that of Pt in the Pt/C. Upon increasing the FePc/carbon mass ratio above 1:1 in the FePc/CB-EC600 composites, the ORR activity decreased. This should be due to that individual FePc aggregates formed at high FePc/carbon mass ratios; and the amounts of the adsorbed FePc molecules in the composites decreased under the same mass of composites.

As for the FePc/GS composites, the 1:1 FePc/carbon mass ratio gave the best ORR performance; while the deviation of FePc/carbon mass ratio from 1:1 led to significant decline of ORR activity (Fig. S8). As implied from the morphology observation discussed above, FePc molecules in the FePc/GS composites were predominantly self-assembled into nanorod aggregates on GS, instead of forming molecular adsorption layers. The catalytic utilization of FePc in the aggregates should be lower than those in the adsorption layer; therefore, higher FePc contents were required to achieve the best ORR activity as GS were used as support. The decrease in the ORR activity with increasing the FePc/carbon mass ratio above 1:1 in the FePc/GS composites should be due to the agglomeration of the FePc nanorods, which could decrease the utilization of FePc.

For practical application, a robust ORR electrocatalyst with high durability and methanol tolerance is of very importance. Fig. 6 compares the chronoamperometric responses (current-time curves) of the two composites and Pt/C at ORR potentials in O_2-saturated solution with and without methanol. In the absence of methanol, the carbon-supported FePc composites were much more stable in maintaining the activity with the evolution of time than the Pt/C (Fig. 6a). As shown in Fig. 6b, no obvious change in the ORR current was observed for the FePc/CB-EC600 and FePc/GS composites upon adding the methanol to the solution; while immediate current diminishing occurred for Pt/C. These results suggested that the FePc-based catalysts were much more durable than Pt/C when acting as the ORR electrocatalysts. It is known that Pt may suffer from oxidation-induced dissolution under the ORR conditions.[30] Besides, Pt is easily poisoned by organic contaminants in the working media. In methanol-contained solution, for example, CO produced from methanol decomposition can be strongly adsorbed on Pt surface. These should be responsible for the activity degradation of Pt/C during the ORR. The Me-N based non-previous metal electrocatalysts mostly don't strongly adsorb small molecules such as CO and methanol.[31] Therefore, they are much tolerant to the organic contaminants. In addition, as indicated by UV-Vis and XPS results, there are relatively strong interaction between FePc and carbon supports, which should provide an anchoring force to stabilize the FePc molecules on the supports.

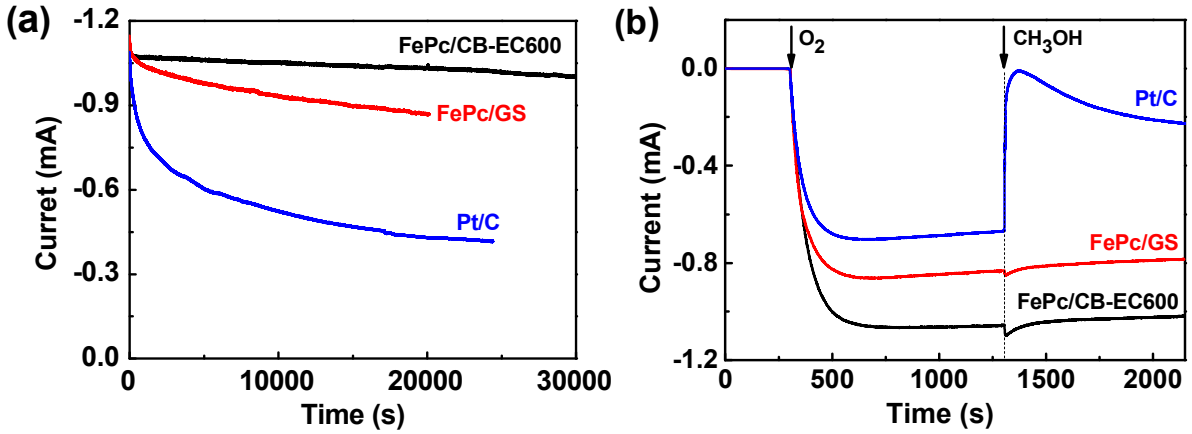

Fig. 6 (a) Current-time curves obtained at the constant potential of 0.7 V in O_2-saturated 0.1 M KOH and (b) that obtained at the constant potential 0.8 V in 0.1 M KOH. The arrows in (b) indicate the introduction of O_2 and methanol in the solution. The electrodes were rotated at a speed of 1600 rpm.

3. Conclusion

Composites of FePc supported on different nanocarbon materials have been prepared using a facile

wet ball-milling method. The assembling behaviors of FePc molecules in the FePc/carbon composites depend on the specific surface areas of the carbon supports, the FePc/carbon mass ratios and the molecule-support interaction. In general, FePc molecules tend to be self-assembled into nanorod aggregates in the course of ball-milling. The presence of 2-D GS can significantly prevent the FePc nanorods from agglomerating. The high specific surface area of CB-EC600 and the strong molecule-support interaction make FePc form uniform adsorption shell on CB-EC600 particles at FePc/carbon mass ratio up to 1:1, which corresponds to nearly two molecular layers of FePc on CB particles. Both of the FePc/GS and FePc/CB-EC600 composites can catalyze the ORR much more efficiently than the state-of-the-art Pt/C catalyst in alkaline solution. Especially, the FePc/CB-EC600 composites with FePc/carbon mass ratios from 1:2 to 1:1 exhibit mass activity of FePc which is 2-3 times higher than that of Pt in Pt/C. As well as showing that the nanocarbon support can provide a degree of control on the molecular architectures of metal macrocyclic compounds, the present work also demonstrates that the FePc molecule is intrinsically more efficient than Pt in catalyzing the ORR, and therefore has great prospect as cathode electrocatalyst in alkaline fuel cells.

4. Experimental Section

4.1 Chemicals and equipments

The 20 wt.% Pt/C and FePc were purchased from Johnson Matthey corporation and Alfa Aesar, respectively.

The model of the ball mill is Mini-Mill Pulverisette 23 provided by Fritsch in Germany. The size of the jar is 10 mL. Additionally, there are three balls with the size of ~5 mm and the material of the ball is stainless steel. The weight of the three balls is about 1.8 g.

4.2 Materials preparation

The graphene nanosheets used in this work were prepared with high temperature thermal reduction of home-made graphene oxide (GO)[32, 33] at 900 ℃ for about 1 hours under high purity argon in a tube furnace.

The carbon-supported FePc composites were prepared by the following procedure. The carbon materials were first mixed with 9 mg of FePc in a desired mass ratio in the presence of ethanol (0.5 mL/mg mixture). Then, the mixture was placed in the jar followed by ball-milling with the rotating speed of 30 oscillations/seconds. The weight ratio of precursor materials to balls was ~1:100. After

about 30 mins' ball-milling, the mixture was transferred into a beaker and dried in a vacuum oven for 24 h. Finally, the dried product was adequately ground to obtain the composite catalysts.

4.3 Physical characterization

Scanning electron microscopy (SEM) images were obtained by a HITACHI S-4800 scanning electron microsope. The images of transmission electron microscope (TEM) were taken using a JEM-2100 and the high resolution TEM (HRTEM) images were probed by a high-resolution field emission transmission electron microscope JEM-2010FEF (UHR) (Center for Electron Microscopy Wuhan University). X-ray photoelectron spectroscopy (XPS) measurements were performed using a Kratos Ltd. XSAM-800 spectrometer with a Mg Kα X-ray source, and the data were fitted using the software XPSPEAK41. The N_2 adsorption isotherms of the sample catalysts were investigated using an ASAP2020 surface area and porosity analyzer (Micromeritics, U.S.A.).

4.4 Electrochemical measurements

All of the electrochemical tests were carried out in a standard three-electrode cell using a Pt foil counter electrode and a Hg/HgO reference electrode. The electrochemical cell was controlled with a CHI 440. The ORR measurements were conducted in an O_2-saturated 0.1 M KOH electrolytes with a potential scanning rate of 5 mV/s. To calibrate the reference electrodes to the RHE scale, the RHE zero potential was estimated with the potential at which the current crossed zero by measuring the steady-state polarization curves of the hydrogen electrode reactions on Pt/C-loaded glass carbon disk electrode in 0.1 M KOH saturated with H_2. To load catalyst samples on glass carbon disk electrode, 5 mg catalyst was dispersed in 1 mL solution of Nafion in isopropyl alcohol (1 mL 5 wt% Nafion mixed with 49 mL isopropyl alcohol). 4 μL of the resulting suspension was pipetted onto the glass carbon disk to form a thin catalyst layer, with a catalyst loading of 0.1 mg/cm^2.

The peroxide yield during the ORR and the apparent electrons transferring numbers (n) were calculated based on the following equations:

$$HO_2^- \% = 200I_R/(N*I_D+I_R) \quad \text{(Eq. 1)}$$

$$n=4I_D/[I_D+(I_R/N)] \quad \text{(Eq. 2)}$$

Where I_D and I_R represent the disk and ring currents respectively, and N is the current collection efficiency of the Pt ring, which was 0.25 in our system.

Acknowledgements

This work was supported by the Ministry of Science and Technology of China under the National Basic Research Program (Grant nos. 2012CB215500 and 2012CB932800).

Notes and references

Hubei Key Laboratory of Electrochemical Power Sources, Key Laboratory of Analytical Chemistry for Biology and Medicine (Ministry of Education), Department of Chemistry, Wuhan University, Wuhan 430072, China. Fax: 027-68754693; Tel: 027-68754693; E-mail: slchen@whu.edu.cn

† Electronic Supplementary Information (ESI) available: additional electron microscopy images, XPS spectra and electrochemical results. See DOI: 10.1039/b000000x/

1 M. K. Debe, *Nature*, 2012, **486**, 43-51.

2 A. Morozan, B. Jousselme and S. Palacin, *Energy Environ. Sci.*, 2011, **4**, 1238-1254.

3 J. Greeley, I. E. L. Stephens, A. S. Bondarenko, T. P. Johansson, H. A. Hansen, T. F. Jaramillo, J. Rossmeisl, I. Chorkendorff and J. K. Nørskov, *Nat. Chem.*, 2009, **1**, 552-556.

4 F. Jaouen, E. Proietti, M. Lefèvre, R. Chenitz, J. P. Dodelet, G. Wu, H. T. Chung, C. M. Johnston and P. Zelenay, *Energy Environ. Sci.*, 2011, **4**, 114-130.

5 Z. Chen, D. Higgins, A. Yu, L. Zhang and J. Zhang, *Energy Environ. Sci.*, 2011, **4**, 3167-3192.

6 R. Jasinski, *Nature*, 1964, **201**, 1212-1213.

7 H. Jahnke, M. Schönborn and G. Zimmermann, *Top. Curr. Chem.*, 1976, **61**, 133-181.

8 S. Yamazaki, Y. Yamada, T. Ioroi, N. Fujiwara, Z. Siroma, K. Yasuda and Y. Miyazaki, *J. Electroanal. Chem.*, 2005, **576**, 253-259.

9 P. Gouérec and M. Savy, *Electrochim. Acta*, 1999, **44**, 2653-2661.

10 U. I. Koslowski, I. Abs-Wurmbach, S. Fiechter and P. Bogdanoff, *J. Phys. Chem. C*, 2008, **112**, 15356-15366.

11 G. Wu and P. Zelenay, *Acc. Chem. Res.*, 2013, **46**, 1878-1889.

12 M. Lefèvre, E. Proietti, F. Jaouen and J.-P. Dodelet, *Science*, 2009, **324**, 71-74.

13 H. Shi, Y. Shen, F. He, Y. Li, A. Liu, S. Liu and Y. Zhang, *J. Mater. Chem. A*, 2014, **2**, 15704-15716.

14 R. Baker, D. P. Wilkinson and J. Zhang, *Electrochim. Acta*, 2008, **53**, 6906-6919.

15 S. A. Mamuru, K. I. Ozoemena, T. Fukuda, N. Kobayashi and T. Nyokong, *Electrochim. Acta*, 2010, **55**, 6367-6375.

16 R. Chen, H. Li, D. Chu and G. Wang, *J. Phys. Chem. C*, 2009, **113**, 20689-20697.

17 R. Cao, R. Thapa, H. Kim, X. Xu, M. G. Kim, Q. Li, N. Park, M. Liu and J. Cho. *Nat. Commun.*, 2013, **4**, 2076 (1-7).

18 H. Tang, H. Yin, J. Wang, N. Yang, D. Wang and Z. Tang, *Angew. Chem. Int. Ed.*, 2013, **52**, 5585-5589.

19 P.-J. Wei, G.-Q. Yu, Y. Naruta and J.-G. Liu, *Angew. Chem. Int. Ed.*, 2014, **53**, 6659-6663.

20 Y. Jiang, Y. Lu, X. Lv, D. Han, Q. Zhang, L. Niu and W. Chen, *ACS Catal.*, 2013, **3**, 1263-1271.

21 E. Yoo and H. Zhou, *J. Power Sources*, 2013, **244**, 429-434.

22 I. Kruusenberg, L. Matisen, Q. Shah, A. M. Kannan and K. Tammeveski, *Int. J. Hydrogen Energy*, 2012, **37**, 4406-4412.

23 I. Kruusenberg, J. Mondal, L. Matisen, V. Sammelselg and K. Tammeveski, *Electrochem. Commun.*, 2013, **33**, 18-22.

24 J.-H. Yang, Y. Gao, W. Zhang, P. Tang, J. Tan, A.-H. Lu and D. Ma, *J. Phys. Chem. C*, 2013, **117**, 3785-3788.

25 H. Wang and H. Dai, *Chem. Soc. Rev.*, 2013, **42**, 3088-3113.

26 P. Borghetti, A. El-Sayed, E. Goiri, C. Rogero, J. Lobo-Checa, L. Floreano, J. E. Ortega and D. G. Oteyza, *ACS Nano*, 2014, **8**, 12786-12795.

27 Y. Zhang, K. Fugane, T. Mori, L. Niu and J. Ye, *J. Mater. Chem.*, 2012, **22**, 6575-6580.

28 Y. Nabae, S. Moriya, K. Matsubayashi, S. M. Lyth, M. Malon, L. Wu, N. M. Islam, Y. Koshigoe, S. Kuroki, M.-A. Kakimoto, S. Miyata and J.-I. Ozaki, *Carbon*, 2010, **48**, 2613-2624.

29 L. Gan, R. Yu, J. Luo, Z. Cheng and J. Zhu, *J. Phys. Chem. Lett.*, **2012**, *3*, 934-938.

30 F. Tian and A. B. Anderson, *J. Phys. Chem. C*, 2008, **112**, 18566 -18571.

31 W. L. Queen, M. R. Hudson, E. D. Bloch, J. A. Mason, M. I. Gonzalez, J. S. Lee, D. Gygi, J. D. Howe, K. Lee, T. A. Darwish, M. James, V. K. Peterson, S. J. Teat, B. Smit, J. B. Neaton, J. R. Longci and C. M. Brown, *Chem. Sci.*, 2014, **5**, 4569-4581.

32 S. Zhang, H. Zhang, Q. Liu and S. Chen, *J. Mater. Chem. A*, 2013, **1**, 3302-3308.

33 S. Zhang, B. Liu and S. Chen, *Phys. Chem. Chem. Phys.*, 2013, **15**, 18482-18490.

TOC

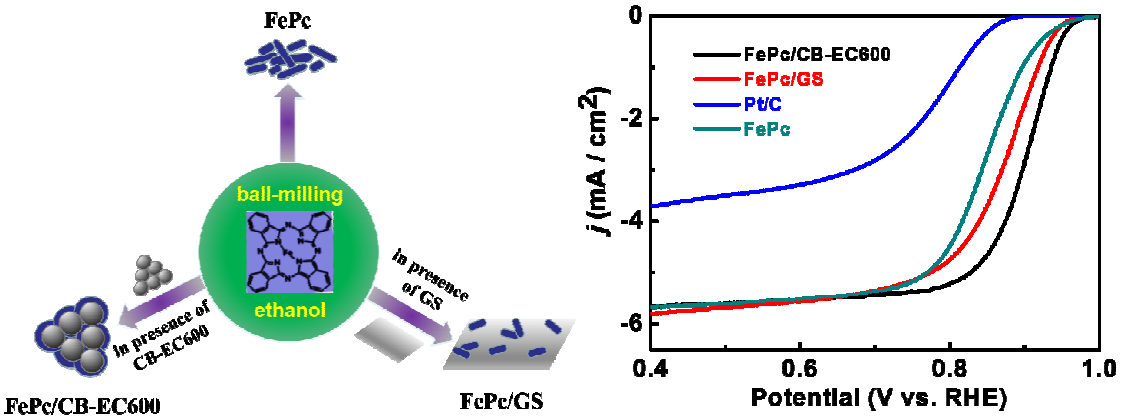

Tailored molecular architectures of FePc on nanocarbon supports from nanorods to uniform shells exhibit excellent electrocatalytic activity for the oxygen reduction reaction in alkaline solution.